

Reduced cloud cover errors in a hybrid AI-climate model through equation discovery and automatic tuning

Arthur Grundner^{1,*}, Tom Beucler^{2,3}, Julien Savre¹, Axel Lauer¹,
Manuel Schlund¹, Veronika Eyring^{1,4}

¹Deutsches Zentrum für Luft- und Raumfahrt e.V. (DLR), Institut für Physik der Atmosphäre, Oberpfaffenhofen, Germany

²Faculty of Geosciences and Environment, University of Lausanne, Lausanne, Switzerland

³Expertise Center for Climate Extremes, University of Lausanne, Lausanne, Switzerland

⁴University of Bremen, Institute of Environmental Physics (IUP), Bremen, Germany

*Corresponding author: arthur.grundner@dlr.de

Abstract

Cloud-related parameterizations remain a leading source of uncertainty in climate projections. Although machine learning holds promise for Earth system models (ESMs), many data-driven parameterizations lack interpretability, physical consistency, and smooth integration into ESMs. Here, a two-step method is presented to improve a climate model with data-driven parameterizations. First, we incorporate a physically consistent cloud cover parameterization—derived from storm-resolving simulations via symbolic regression, preserving interpretability while enhancing accuracy—into the ICON global atmospheric model. Second, we apply the gradient-free Nelder–Mead optimizer to automatically recalibrate the hybrid model against Earth observations, tuning in nested stages (2-, 7-, 30- and 365-day runs) to ensure stability and tractability. The tuned hybrid model substantially reduces long-standing biases in cloud cover—particularly over the Southern Ocean (by 75%) and subtropical stratocumulus regions (by 37%)—and remains robust under +4K surface warming. These results demonstrate that interpretable machine-learned parameterizations, paired with practical tuning, can efficiently and transparently strengthen ESM fidelity.

Introduction

When digitally modeling the dynamics of a physical field, it needs to be overlaid by a discrete grid. Processes that are happening inside individual grid cells and thus cannot be resolved may

have a significant impact on the overall dynamics and must therefore be inferred from the available grid-scale information. In climate models, so-called parameterizations tackle this task¹. It is natural to learn from data where (e.g., process) knowledge is lacking, therefore, the development of data-driven and machine learning based parameterizations has become widespread in recent years^{2,3,4,5,6,7}. Because of their representation power, neural networks are a common choice for data-driven modeling⁸, despite coming with some clear and significant drawbacks: They often deteriorate the interpretability of climate models, making it difficult to prove their physical consistency, they degrade the climate model's applicability to climate change scenarios⁹, and they increase the computational burden when replacing a parameterization that used to be formulated as a simple equation¹⁰.

In the development of all types of data-driven parameterizations, the training and testing of a scheme is performed either ‘offline’ (i.e., in a stand-alone fashion on a reference dataset) or ‘online’ (i.e., implemented in and interacting with the dynamics of a climate model)^{5,11}. Online training requires either a differentiable host climate model¹² or costly inverse methods¹³, making offline training the dominant approach for data-driven parameterizations. However, these offline-trained parameterizations have yet to demonstrate consistent performance online, due to the need for a tuning step to adjust the climate model to its new parameterization^{14,15}. Such a tuning step usually requires a lot of time and expert knowledge. Its execution also becomes less straightforward as deep learning-based parameterizations no longer include such physics-related tunable parameters. Thus, many of the offline-trained models are never tested online, leading to increased doubts about their usefulness for climate modeling¹². After all, it is not obvious that a data-driven parameterization can overcome this ‘optimization dichotomy’¹⁶ of being trained in one setting while expected to perform well in a different setting.

In this paper we do not only demonstrate the strong online skill of our offline-trained, data-driven parameterization, but also introduce a new automatic tuning pipeline that enables these results. More specifically, we consider an *analytical equation* (equation (1)) from Grundner et al.¹⁷ that has been trained offline to parameterize cloud fraction, reducing related systematic model errors towards improved climate projections. The equation was derived from a high-resolution simulation using a symbolic regression library¹⁸ for equation discovery^{19,20}. It is the product of a data-driven approach that provides accuracy and yet retains the interpretability, physical consistency and computational efficiency of the traditional parameterization. However, its application in a climate model has not yet been demonstrated. To do so, we first implement the cloud cover equation into ICON-A²¹, the atmospheric component of the ICOsahedral Non-hydrostatic (ICON) climate model. We then set up an automatic tuning procedure following a multi-objective approach²² to tune the model, hereafter called ‘ICON-A-MLe’ where MLe stands for Machine Learning enhanced. The basic idea is to tune as much as possible using simulations that are as short as possible. Here, we build on the finding that biases resulting from fast physical processes can already be identified in short simulations of a day, week or month²³. Compared to other recent automated tuning methods for climate models (e.g., Bonnet et al.²⁴, Roach et al.²⁵), our tuning procedure is simpler and thus more efficient and better generalizable.

We begin by outlining the tuning pipeline and its impact on ICON-A-MLe model results. We then compare the tuned ICON-A-MLe model with observations, as well as to models participating in the Coupled Model Intercomparison Project Phase 6 (CMIP6²⁶) and to an automatically and manually tuned version of ICON-A. For the evaluation, we perform a historical Atmospheric Model Intercomparison Project (AMIP) simulation from 1979-1999, which has prescribed sea sur-

face temperatures (SSTs) and sea ice concentrations, and evaluate it with Earth observations to assess its accuracy. For this we use the Earth System Model Evaluation Tool (ESMValTool), an established community diagnostic and performance metrics tool for the evaluation and analysis of Earth system models^{27,28,29,30,31,32,33}, recently extended to be able to process ICON output without model postprocessing³⁴. Finally, we demonstrate its robustness by applying ICON-A-MLe to a significantly warmer climate.

Overview of the Automatic Tuning Pipeline

To effectively integrate the data-driven cloud cover equation ((1) in Methods) into ICON-A, we developed a simple and efficient automatic tuning pipeline (Fig. 1). This pipeline uses the Nelder–Mead optimization algorithm to calibrate a set of 24 physical and empirical parameters—spanning cloud microphysics, convection, and the new parameterization (Table S2)—against observationally derived target metrics (Methods).

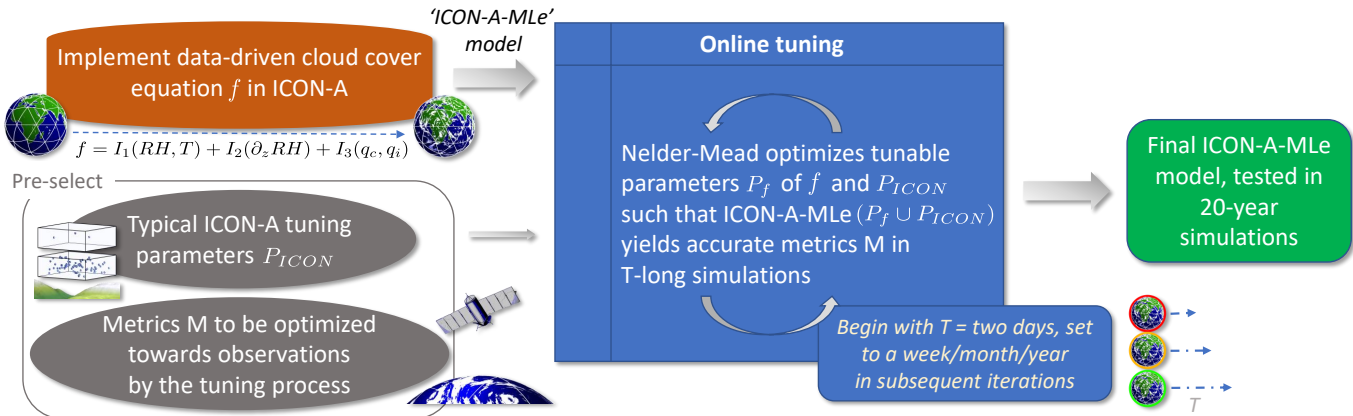


Figure 1: The automatic tuning pipeline of ICON-A-MLe, i.e., the ICON atmospheric climate model including our data-driven cloud cover equation ((1) in Methods). The only manual step involves selecting the climate metrics to be optimized, such as globally averaged cloud cover, and determining which tunable parameters should be adjusted. Reasonable target ranges for these metrics are derived from observational and reanalysis data. The core of the tuning pipeline consists of the Nelder-Mead algorithm iteratively searching for a setting of the tunable parameters that enables ICON-A-MLe simulations to optimize all specified metrics. The length of these simulations and the strictness of evaluating the metrics increases with the number of iterations. The underlying strategy leverages the fact that some climate metrics exhibit rapid responses to parameter changes, allowing for efficient feedback and early adjustments. Finally a historical AMIP simulation is benchmarked to Earth observations with the ESMValTool.

Utilizing computational resources carefully, the tuning process proceeds in stages, beginning with short 2-day simulations and increasing in duration to 7-day, 30-day, and finally 365-day simulations. At each stage, simulation outputs are compared to observational constraints on key global metrics such as the top-of-the-atmosphere (TOA) radiation balance, shortwave (SW)/longwave

(LW) cloud radiative effects, precipitation, and cloud water paths. The objective function guiding optimization quantifies the normalized distance between simulated values and observational ranges. The shorter the simulations in a given stage, the more those ranges are relaxed informed by the typical variability of a given metric in a reference ICON simulation. Each optimization stage refines the parameter space based on the best result from the previous stage. The final step includes an extrapolated parameter update to balance short- and long-term simulation objectives, followed by a small number of year-long simulations to identify an optimal parameter set. This iterative strategy allows for robust and efficient convergence toward physically realistic climate simulations.

Fig. 2 illustrates the impact of the automatic tuning pipeline on the performance of ICON-A-MLe in 20-year simulations for three key radiative metrics (zonal means of the absorbed SW and outgoing LW radiation are provided in Fig. S6). When the data-driven equation (1) with its original parameters (Table S2) is first implemented in ICON, these metrics deviate significantly from observations without tuning. After each optimization stage, these metrics gradually improve with the top-of-the-atmosphere radiative balance assuming realistic values at the end of the tuning process.

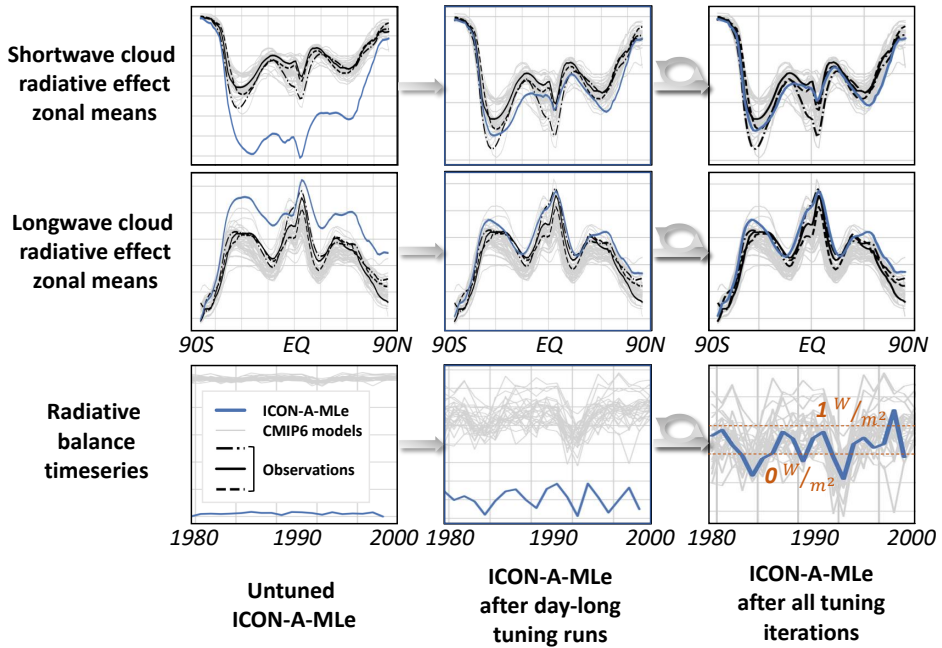


Figure 2: A qualitative evaluation of 20-year ICON-A-MLe simulations using parameter settings extracted at three different stages of the tuning pipeline. The panels display radiative measures computed at the top of the atmosphere, illustrating the model’s progression through the tuning process. Circular arrows denote intermediate tuning steps involving week- and month-long ICON-A-MLe simulations. Observational references are derived from MERRA2³⁵, CERES³⁶, and ISCCP³⁷. The solid gray lines represent historical CMIP6 model simulations²⁶, providing a benchmark for comparison.

Evaluation of 20-year ICON Simulations

In this section, we compare the tuned ICON-A-MLe and ICON-A models with observational reference datasets, focusing on the mean state of the simulated climate. Specifically, we conduct a quantitative evaluation of the 20-year historical AMIP simulations referenced in the green box of Fig. 1.

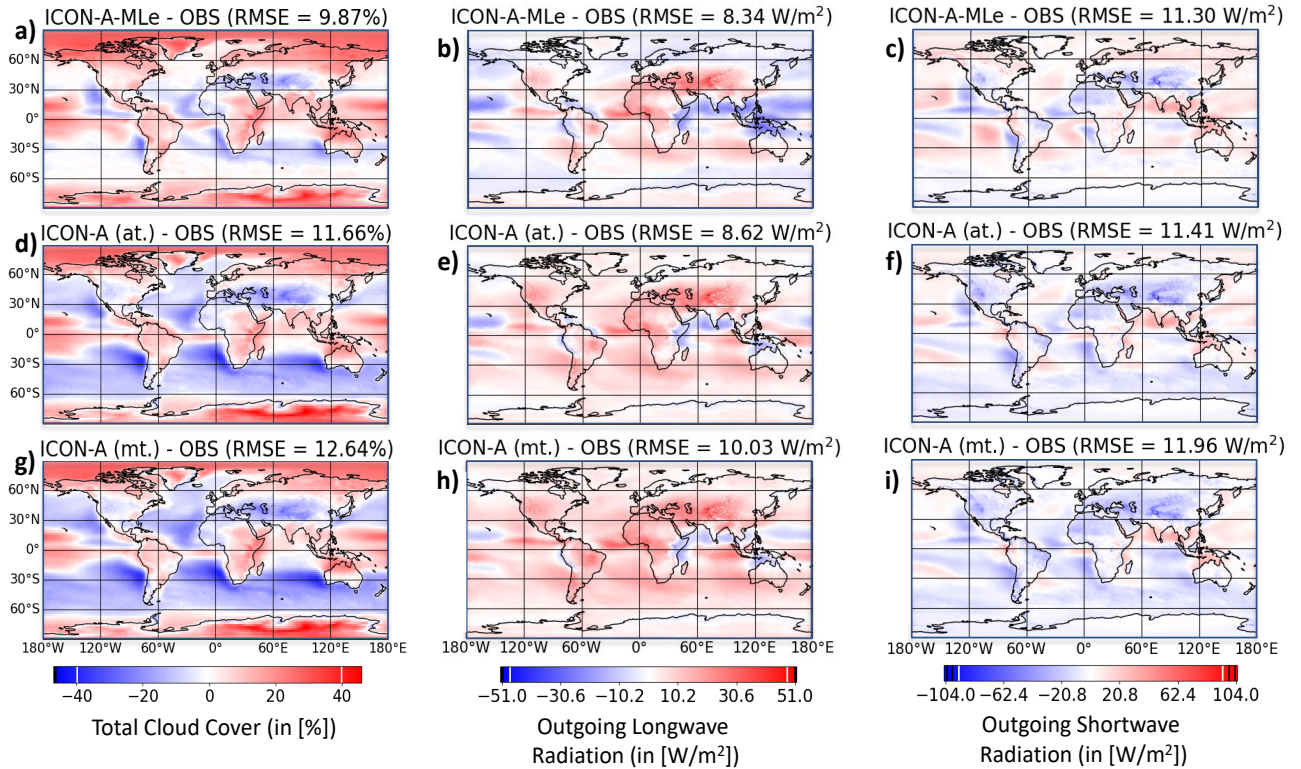


Figure 3: Biases in three key climate metrics, temporally averaged over 20-year simulations (1979–1999), for our automatically tuned (at.) ICON-A-MLe (first row) and ICON-A models (second row), and a manually tuned (mt.) ICON-A reference (third row). Root-mean-square errors (RMSEs) are computed after remapping the data onto a horizontal grid with nearly identical grid cell sizes. The maximum range of values within each panel is indicated by white (for ICON-A-MLe) and black (for ICON-A) vertical lines in the colorbars. To enhance the robustness of our observational reference (OBS), we take an average across multiple observational cloud cover datasets (CLARA-AVHRR³⁸, ESA CCI³⁹, MODIS⁴⁰, PATMOS⁴¹), as well as two reanalysis products (MERRA2³⁵, ERA5⁴²). For radiative metrics, we use ESA CCI³⁹ (1982–1999) and ISCCP³⁷ (1984–1999), as these observations are among the most reliable spanning the majority of the simulated 1979–1999 period.

Total cloud cover is the first metric to evaluate when testing a new cloud cover parameterization. Its importance cannot be overstated: clouds are fundamental to the Earth’s energy budget, as they can either cool the Earth by reflecting sunlight or warm it by trapping heat. Their role in modulating precipitation and humidity further underscores their influence on local and regional climates⁴³.

The first column of Fig. 3 demonstrates that ICON-A-MLe achieves a notably more accurate representation of the geographical distribution of temporally averaged total cloud cover compared to the manually and automatically tuned ICON-A setups (global RMSE reduced by 15.4% from panel d) to a)). These improvements are most evident in maritime regions, particularly in those dominated by marine low-level clouds⁴⁴; the Southern Ocean (RMSE reduced by 75.8%), the west coasts of Chile/Peru (by 49.9%), Namibia/Angola (by 19.5%), California (by 24.1%), Morocco (by 41.8%), and Australia (by 53.3%). These are precisely the regions that exhibit the largest positive differences between panels a) and d) (see Fig. S7 a)). Polewards of 60°N and 60°S, ICON-A significantly overestimates cloud cover. While ICON-A-MLe shows an increased cloudiness over Canada and Greenland even further (locally by up to 23%) compared to ICON-A, it displays reduced cloud cover over most of Antarctica (by nearly 10%), thereby decreasing the corresponding bias to below 40% cloud cover. As the remaining deviation cannot be entirely explained by the substantial measurement uncertainty in polar regions (up to 15%⁴⁵), this motivates further refinement in future studies.

While the cloud cover root-mean-square error (RMSE) is lower for the automatically tuned (panel d) compared to the manually tuned (panel g) ICON-A simulation ($\Delta\text{RMSE} = -0.98 \text{ W/m}^2$), their bias plots are almost indistinguishable as regional differences are typically rather small ($\leq 10\%$ cloud cover as can be seen in Fig S7 d)).

Improvements we find in cloud cover are most valuable if, to some extent, they translate to improved radiative metrics. After all, an accurate representation of LW and SW radiation is crucial for ensuring that the climate model can effectively simulate the Earth's energy budget—a fundamental component for projecting temperature and other climate-relevant parameters. The second column of Fig. 3 reveals that the manually tuned ICON-A (panel h)) generally overestimates outgoing LW radiation, particularly over mountainous regions. This overestimation arises from the model's coarse-resolution grid, which smooths topography and causes mountains appear lower—and therefore warmer—than in reality. The automatically tuned ICON-A (panel e)) shows a reduced outgoing LW radiation globally, except for a localized increase (up to 15 W/m²) around the Philippines (see also Fig. S7 e)). ICON-A-MLe further reduces outgoing LW radiation, bringing it closer (with exceptions over the tropics) to observations. Especially over oceans, the increase in cloud cover causes reduced LW radiation now being emitted from cloud tops that are cooler than the ocean's surface. However, ICON-A-MLe tends to underestimate outgoing LW radiation over the tropical western Pacific. This bias stems partly from a (more accurate) increase in cloud ice (see Fig. S8), which forms at higher altitudes and thus emits less LW radiation.

The difference between the SW radiation maps (third column of Fig. 3) from ICON-A-MLe (panel c)) and the automatically tuned ICON-A (panel f)) are highly correlated with those of cloud cover (see also Fig. S7). The largest discrepancies occur in regions with an abundance of marine low-level clouds, where increased cloud coverage leads to more SW radiation being reflected back to space. The increase in cloudiness turns a slight underestimation of the reflected TOA SW radiation into a slight overestimation and results in a small global RMSE improvement ($\Delta\text{RMSE} = -0.11 \text{ W/m}^2$). Meanwhile, the automatically tuned ICON-A's SW radiation map itself shows improvements ($\Delta\text{RMSE} = -0.55 \text{ W/m}^2$) over the manually tuned version due to its increased marine low-level cloud coverage and consequently increased reflected SW radiation. Across all three metrics—cloud cover, outgoing LW, and reflected SW radiation—ICON-A-MLe consistently achieves the lowest RMSE values, while the manually tuned ICON-A model performs the worst. This underscores the improvement that can be achieved through the combination of the automatic tuning

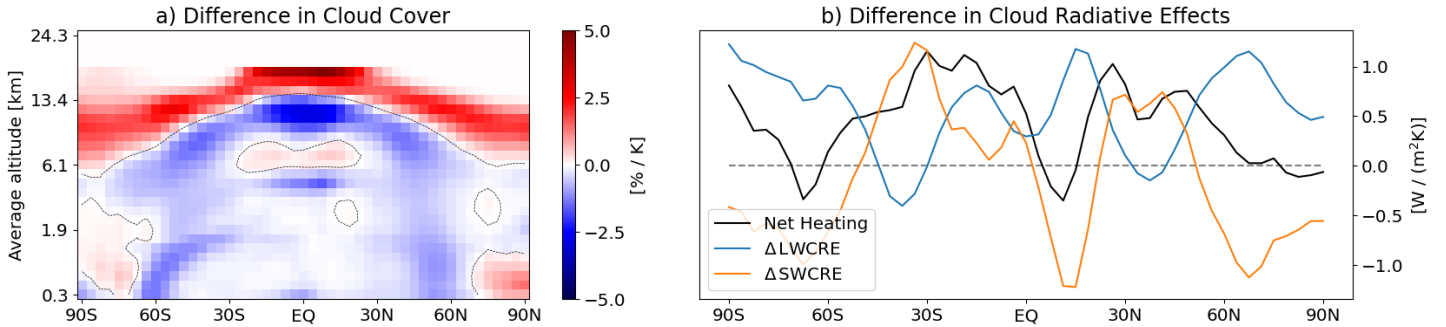


Figure 4: Application of our ICON-A-MLe model in a sea surface temperature increase scenario of +4 K: Panel a) illustrates the changes in cloud cover per degree of warming as a function of latitude and altitude relative to a control simulation without induced heating. Dashed contour lines are indicating 0 %/K. Panel b) presents the corresponding changes in longwave (LW) and shortwave (SW) cloud radiative effects (CRE), and the net cloud-induced heating, i.e., $\Delta\text{LWCRE} + \Delta\text{SWCRE}$, as a function of latitude. Both metrics are computed over the last 10 years of a 20-year simulation (1979–1999) and are normalized by the imposed sea surface temperature increase (4 K).

procedure and the data-driven cloud cover equation.

In addition to the three metrics presented in Fig. 3, Table S1 provides a comprehensive comparison of the biases (RMSE and R^2 -values) for other key climate variables across the three simulations. While minor increases in RMSE can occur, the R^2 -values of ICON-A-MLe are consistently on par with or better than those of the ICON-A models (with the exception of ice water path being slightly better in the manually tuned ICON-A with $\Delta R^2 = -0.02$). The most striking improvement ($\Delta R^2 = 0.22$) is observed in the liquid water path, defined as the vertically integrated amount of cloud water.

Application of ICON-A-MLe to Warmer Climates

For a climate model to provide reliable future climate projections, it must respond reasonably to changes in climate conditions. To assess the applicability of ICON-A-MLe to a warmer climate, we increase the SST uniformly by 4 K, following a common proxy for global warming scenarios^{8,46,47}. Using the same model setup as in the previous section, we perform a 20-year +4 K simulation with ICON-A-MLe. Figure 4 evaluates only the last 10 years of the simulation to allow for model adjustment to the increased SST.

The +4 K simulation exhibits a notable rise in the cloud top heights across all latitudes, particularly in the tropics (panel a)). This lifting is expected due to a deepening of the troposphere, consistent with observational evidence^{48,49}. The depicted decrease of low-level cloud cover at low to mid-latitudes is a direct consequence of increased SSTs, aligning with many current climate model projections⁵⁰. This effect is more pronounced at 60°S than at 60°N due to the absence of landmasses in the Southern Hemisphere. Over the Arctic, ICON-A-MLe simulates an increase in low-level clouds under the +4 K scenario, in agreement with observations⁵¹ and the CESM1 cli-

mate model⁵². This increase is attributed to sea ice loss during fall. Overall, simulated total cloud cover decreases by 1.65% in the +4 K scenario. A reduction in total cloud cover with warming is expected, primarily due to the Clausius-Clapeyron relationship⁵³.

Panel b) presents the difference in cloud radiative effects between the +4 K and the control simulations, separated into SW and LW components. A positive $\Delta\text{LWCRE}/\Delta\text{SWCRE}$ indicates that changes in cloudiness warm the troposphere in the +4 K simulation. The panel shows that the LWCRE of clouds generally increases in the +4 K simulation due to higher and thus colder cloud tops, which emit less LW radiation. Additionally, LWCRE changes are sensitive to the altitude at which cloud cover changes occur. The reduction in low-level cloud cover at 60°S/60°N has very little impact on the warming effect of clouds, whereas decreases in mid-level clouds at 40°S, the Equator, and at 40°N lead to a noticeable reduction in ΔLWCRE . Interpreting the SWCRE differences is more nuanced, as cloud radiative effects are influenced not only by cloud cover but also by cloud optical properties. Given the changes in panel a), one might expect a symmetric ΔSWCRE pattern around the Equator; however, small differences in cloud cover contribute to a significantly reduced albedo effect and increased heating south of the Equator. The observed decrease in the amplitude of SWCRE at 60°S matches the substantial reduction in marine low-level cloud cover. In the Arctic, changes in SWCRE and LWCRE largely offset each other, while in Antarctica, an increase in high-level clouds enhances the positive net cloud radiative effect. Overall, cloud cover changes in the +4 K simulation contribute to a net increase in tropospheric heating by 0.53 W/(m²K).

Conclusion

In this study, we present the first application of a machine-learning based parameterization significantly reducing the persistent cloud cover biases in marine stratocumulus regions (by 24.1–75.8%) in a global climate simulation. We show strong online skill of an offline-trained, data-driven yet physically constrained and interpretable parameterization for cloud cover (Equation 1) alongside a pipeline for automatically calibrating the resulting hybrid climate model with Earth observations. The data-driven cloud cover parameterization, derived via symbolic distillation from high-resolution data, introduces no additional computational burden and maintains the interpretability of the climate model—distinguishing it from many other machine learning-based approaches. The parameterization is implemented into a climate model (ICON-A) and an automatic tuning procedure is used to optimize the performance of the resulting ICON-A-MLe model against observations. Our tuning approach progressively increases the duration of ICON-A-MLe simulations to keep the required computational resources low. The method is characterized by its simplicity, speed (at the expense of quantifying parameter uncertainty), and extensibility to other parameters and metrics. The tuned ICON-A-MLe model substantially reduces long-standing biases in cloud cover and associated radiative fluxes, particularly in regions dominated by low-level clouds (e.g., the Southern Ocean). More broadly, ICON-A-MLe matches or outperforms the original ICON-A model across a wide range of climate metrics. When subjected to +4 K surface warming, the model captures physically plausible changes in cloud cover and cloud radiative effects—a crucial step towards improving climate projections.

While for benchmarking purposes this study focuses on ICON 2.6.4, we anticipate that both the tuning pipeline and the data-driven cloud cover parameterization would yield similar improve-

ments in newer ICON versions or other climate models. Additional enhancements to the tuning procedure could include verifying model performance in different seasons by varying initialization dates before extending to longer simulation periods. Additional metrics and parameters—such as those related to climate system dynamics (e.g., orographic drag or surface wind stress;²¹)—could be added to further calibrate the model. Regarding the representation of cloud cover in ICON-A, data-driven equations for cloud inhomogeneity and overlap may be beneficial.

We emphasize that our approach—discovering a new data-driven equation that can be used as a parameterization and tuning the hybrid climate model—is not specific to the parameterization of cloud cover. Given an appropriate training set, this pipeline can be applied to any parameterization of “fast processes” that one aims to model with a low-dimensional analytical equation. Thus, this work presents a framework for improving climate models using data-driven methods in a practical, computationally efficient, and interpretable way towards hybrid climate models with reduced errors that can provide more robust climate projections for mitigation and adaptation assessments.

Methods

Tuning the ICON Climate Model

In this work we use ICON 2.6.4, a recent version of the ICON climate model with parameterizations still closely based on ECHAM physics (as in Giorgetta et al.²¹). We conduct atmosphere-only simulations at a horizontal resolution of 80 km with a model time step of 10 minutes, a radiation time step of 2 hours, a vertical grid extending up to 83 km across 47 levels, initialization on Jan 1, 2016, relabeled to 1979 (as in Giorgetta et al.²¹), and boundary data (e.g., aerosol and ozone concentrations) matching the simulated date. As a first step, we establish a reliable baseline that we can compare to and build upon.

Manually Tuned Baseline

Our default ICON-A 2.6.4 setup operates on a horizontal grid with increased resolution compared to its original description in Giorgetta et al.²¹, and has seen numerous model changes without being recalibrated. As a consequence, a reasonable top-of-the-atmosphere (TOA) radiative balance (difference between incoming and outgoing radiative fluxes) can only be achieved at the cost of overestimating both TOA net incoming shortwave (SW) and outgoing longwave (LW) radiative fluxes (see Fig. S1). Moreover, total cloud cover is underestimated (global average of 59.3%), which is too small to be deemed acceptable according to Mauritsen et al.⁵⁴. To address these issues, we also manually tuned ICON-A parameters as an additional reference. Specifically, we varied 13 tuning parameters and utilized approximately 300 simulations from Bonnet et al.²⁴, most of them simulating 10 years, to identify which parameters effectively serve as tuning parameters for the radiative metrics and cloud cover (Fig. S2). Key parameters identified through this process are the coefficient of sedimentation velocity of cloud ice (*cvtfall*), entrainment rate for mid-level convection (*entrmid*), and critical relative humidity for condensation in the upper troposphere (*crt*). By decreasing *cvtfall* from 2.5 to 2.25, allowing ice particles to remain suspended in clouds for longer, slightly increasing *entrmid* from 2e-4 to 2.1e-4 and decreasing *crt* from 0.8 to 0.79, enhancing the formation of high-level clouds at lower relative humidities, we could increase global mean total

cloud cover to above 60% (Fig. S1). Additionally, these adjustments yielded SW and LW radiative fluxes at the TOA and a radiative balance, both in close agreement with observations. A comprehensive evaluation of the simulation also demonstrates very reasonable zonal means across various metrics (Fig. S3). By making the convenient yet improper assumption that the impacts of any parameter on a climate metric are linear and independent, we could thus use traditional sensitivity tests to establish a baseline. However, this methodology is both expensive and luck-dependent, highlighting the need for an alternative tuning approach.

Automatic Tuning Pipeline

We hereby introduce a new automatic tuning pipeline (Fig. 1), which we use to tune both the ICON-A baseline model and our ICON-A-MLE model. First, we replace the original cloud cover scheme⁵⁵ in ICON-A 2.6.4 by the data-driven equation (1) for cloud cover from Grundner et al.¹⁷, which showed superior skill in a comprehensive offline evaluation. We then define which model parameters are to be adjusted in the tuning process. Their initial values match those obtained from the manually tuned baseline. Specifically, we target 24 different tuning parameters (listed in Table S2) with a focus on clouds and convection. Ten of the parameters are part of the cloud cover equation and the other 14 are included in the convection (3), cloud optical properties (8), microphysics (2), and vertical diffusion (1) schemes. Our goal is to tune these parameters such that key climate metrics from model simulations are in good agreement with observations. We therefore specify these 24 parameters as inputs to an optimization method, whose objective (function) value quantifies the deviation of a climate model simulation that is based on a specific realization of these parameters from observational reference data. As optimization method we use the Nelder-Mead (NM) method (also called ‘downhill simplex method’)⁵⁶, which is efficient and does not require differentiation of the objective function. To find a minimum, the NM method moves a simplex through the parameter space, iteratively running the ICON model and evaluating the objective function (i.e., the deviation of a model simulation from the reference data) using the parameter values corresponding to each vertex of the simplex in every step.

To minimize the use of computational resources, we start by simulating only two days. After the NM algorithm has finished tuning the parameters such that the corresponding simulation is as close to the reference data as possible (in practice, when either the objective value is zero or a runtime of 8 hours is reached), we extend the simulation duration to a week, then a month, and finally a year. In each iteration with a given ICON simulation duration, the parameters are initialized using the best setting of the previous iteration. In the last iteration, we avoid multiple full NM cycles using expensive year-long simulations. Instead, we first perform a single NM cycle using a limited number (14–20) of year-long simulations, constrained by the 8-hour runtime limit. This yields a set of candidate parameter vectors, from which we select the one that minimizes the objective function, denoted P_{\min} , along with its associated TOA energy balance loss, T_{\min} . In parallel, we retain the best parameter set P_{month} , from the previous NM tuning step that used month-long simulations, along with its corresponding TOA loss T_{month} . We then construct a new candidate parameter vector P by extrapolating between P_{month} and P_{\min} . Specifically, we set

$$P = P_{\text{month}} - \frac{T_{\text{month}}}{T_{\min} - T_{\text{month}}} (P_{\min} - P_{\text{month}}),$$

such that the expected TOA loss is minimized under a linear approximation.

A second NM cycle is then performed around this extrapolated parameter vector, again using 14–20 year-long simulations. If any of these runs produce a TOA imbalance in the desirable range of 0.5 to 1 W m^{-2} , we select the best among them (with the lowest objective value) even if this value is up to 25% worse than the global minimum. Thereby, we prioritize the TOA balance when sufficiently good solutions are found. Otherwise, we select the parameter set with the lowest objective value. This strategy typically yields high-quality solutions while limiting the number of costly year-long simulations to fewer than 40.

How do we measure the deviation of a model simulation from given reference data? First, we define a set of metrics (denoted as \mathbf{M} in Fig. 1) consisting of globally and temporally averaged (excluding the first day) outgoing TOA LW and SW radiation, the balance between incoming and outgoing radiation, SW and LW cloud radiative effects (CRE), total cloud cover, precipitation, ice and liquid water paths, and water vapor path. Additionally, we consider total cloud cover in the Southeastern Pacific [15–45°S, 75–105°W] (averaging at 0.71), a proxy for representing subtropical stratocumulus clouds, that are typically underestimated in climate models. The LWCRE/SWCRE is defined here as the difference between the TOA outgoing LW/SW radiation in clear-sky conditions and the all-sky (actual) outgoing LW/SW radiation. We then assess whether the simulated metrics fall within the respective ranges provided by multiple observational products (e.g., from CERES³⁶, GPCP-SG⁵⁷, and ISCCP³⁷). The contribution of each metric to the objective value is quantified as the distance between its computed value and the observational range, normalized by the range width to ensure a relative comparison.

Based on the observational products, the expected ranges for outgoing LW and SW radiation are [231, 242] and [100, 110] W/m^2 , respectively, while the net radiation balance should fall within [0.5, 0.9] W/m^2 . Precipitation is expected to range from [2.7, 3.0] mm/day, whereas bounds for the remaining metrics are taken from Lauer et al.⁵⁸, Table 5. These bounds are derived from annual means over at least 20 years within the period 1980–2020, and are systematically relaxed (by adding a variability score to the upper bound and subtracting it from the lower bound) for shorter simulations to account for natural variability. This variability score is estimated by first averaging standard ICON-A model outputs over periods matching the current simulation length, and by then taking the differences between a metric’s most extreme values and its average value. Without such an adjustment of the bounds, shorter simulations would be excessively constrained, limiting the effectiveness of the tuning method. The degree of relaxation varies by metric and simulation length. For example, for global precipitation, the relaxed bounds are [2.34, 3.42], [2.48, 3.23], [2.57, 3.18], and [2.67, 3.03] mm/day for daily, weekly, monthly, and yearly averages, respectively. Note that the required relaxation is relatively small for this metric, as the daily average of global precipitation is already a good approximation of its long-term mean.

How does the tuning pipeline improve the climate model and affect parameter values? At the start of the first tuning iteration, using day-long ICON-A-MLE simulations, cloud cover and cloud water are strongly overestimated, negatively affecting the SW radiative budget and inducing errors in the related tuning metrics (Fig. 2). These issues are largely resolved halfway through the iteration, most notably through a substantial reduction in the cloud cover offset (by 32.6%; a_1 in equation (1) and Table S2). Towards the end of the iteration, a_1 is increased even above its initial value and a remaining underestimation of the water vapor path is corrected through fine-tuning of

all parameter values, decreasing the objective value to zero (see also Fig. S4). The second column of Fig. 2 shows that a 20-year simulation using the parameter values refined in the first iteration already shows substantial improvements in the three radiative metrics, although the radiative balance has not yet been achieved. Such a discrepancy is expected at this stage, as the parameters have only been tuned to produce accurate single-day results so far.

As the automated tuning process progresses, gradually increasing the ICON-A-MLe simulation duration, the model’s skill continues to improve. Eventually, the TOA radiative balance—whose observational estimate lies between 0 and 1 W/m²—falls within the range of CMIP6 model results. While an objective value of zero is quickly attained in tuning iterations using week- and month-long simulations, in year-long simulations it is decreased from 2.42 to 1.77 (see also Fig. S5). A final loss of zero is difficult to attain as it requires a full reconciliation of high total cloud cover over the Southeast Pacific with an accurate TOA radiative budget.

Table S2 details the parameter modifications due to tuning, with the parameters of the data-driven cloud cover equation (1) listed first. Besides the reduction in the cloud cover offset, notable changes include a slight increase in cloud cover sensitivity to relative humidity and temperature, as well as a 42% decrease in the numerical stabilizer ϵ , which discourages the formation of unrealistic condensate-free clouds. Dependencies on cloud water/ice and vertical relative humidity gradients remain largely unchanged, reinforcing their role in representing thin marine stratocumulus clouds in the model. Adjustments in other parameterizations include setting the Prandtl number slightly above 1 (1.02), modifying cloud droplet number concentrations at low altitudes, and increasing cloud inhomogeneity factors for most cloud types.

In general, we find that it is beneficial to modify many parameters slightly, which is difficult to achieve manually. We find that those parameters that undergo significant changes already do so in the first tuning iteration with day-long simulations (e.g., $cn2sea$ is changed from 80 to 41.71). In subsequent iterations, parameter adjustments typically become smaller and tend to stabilize. Exceptions include the numerical stabilizer, which is further reduced in the month-long iteration (from 0.80 to 0.62).

The overall computational cost of tuning the ICON-A-MLe model automatically amounts to approximately 400 node-hours (using 12 AMD EPYC 7763 MILAN CPU nodes in parallel), running 741/29/32/28 ICON-A-MLe simulations in the tuning iterations using daily/weekly/monthly/yearly simulations, respectively.

Automatic tuning of the ICON-A baseline. To ensure maximum comparability between the ICON-A-MLe and ICON-A models, we apply the same automatic tuning approach to the ICON-A baseline. For comparison, tuning the ICON-A baseline does not yield any single dominant parameter modification. Some parameters that were decreased in the ICON-A-MLe tuning (e.g., mid-level entrainment rate, autoconversion of cloud droplets to rain) are instead increased, suggesting a dependency on the cloud cover scheme and demonstrating Nelder-Mead’s ability to adjust parameters accordingly. A notable modification is an increase of the critical relative humidity at the top (by 3.4%) in the iteration with weekly simulations, which reduces the simulated amount of high clouds, correcting an issue of overestimated outgoing SW radiation (reducing it by 1.8 W/m²). In the case of the ICON-A baseline we found that by nudging the critical relative humidities for cloud formation (from 0.99 to 0.968 at the top and from 0.59 to 0.665 at the bottom of the atmosphere) before the second NM cycle, we end up with a slightly better ICON-A model configuration (TOA loss of zero and an objective value of 3.52 instead of 3.78 without the adjustment).

Throughout the tuning process, the challenge of balancing high total cloud cover over the Southeast Pacific with an accurate TOA radiative budget remains more evident in the traditional atmospheric model. Therefore, the total computational cost is higher, amounting to approximately 600 node-hours, with 432/327/158/36 ICON-A simulations in the four tuning iterations.

Data-Driven Cloud Cover Equation

The data-driven equation for cloud cover from Grundner et al.¹⁷, discovered with symbolic regression¹⁸ on coarse-grained data from storm-resolving DYAMOND simulations^{59,60}, can be formulated as follows:

$$f(\text{RH}, \text{T}, \partial_z \text{RH}, q_c, q_i) = I_1(\text{RH}, \text{T}) + I_2(\partial_z \text{RH}) + I_3(q_c, q_i), \quad (1)$$

a function of relative humidity (RH), its vertical derivative ($\partial_z \text{RH}$), temperature (T), cloud water (q_c), cloud ice content (q_i) with

$$\begin{aligned} I_1(\text{RH}, \text{T}) &= a_1 + a_2(\text{RH} - \bar{\text{RH}}) + a_3(\text{T} - \bar{\text{T}}) \\ &+ \frac{a_4}{2}(\text{RH} - \bar{\text{RH}})^2 + \frac{a_5}{2}(\text{T} - \bar{\text{T}})(\text{RH} - \bar{\text{RH}}) \\ I_2(\partial_z \text{RH}) &= a_6^3 \left(\partial_z \text{RH} + \frac{3a_7}{2} \right) (\partial_z \text{RH})^2 \\ I_3(q_c, q_i) &= \frac{-1}{q_c/a_8 + q_i/a_9 + \epsilon}. \end{aligned}$$

After automatically tuning equation (1) online within ICON-A, its attained parameter values are

$$\{a_1, \dots, a_9, \epsilon\} = \{0.118, 1.234, -0.0265 \text{ K}^{-1}, 5.65, 1.56 \cdot 10^{-3} \text{ K}^{-2}, \\ 591.68 \text{ m}, 2.22 \text{ km}^{-1}, 1.47 \text{ mg/kg}, 0.344 \text{ mg/kg}, 0.615\}$$

(see also Table S2). The values for the reference relative humidity $\bar{\text{RH}}$ (0.6025) and temperature $\bar{\text{T}}$ (257.06 K) are fixed.

Data availability

Algorithms, code, and data for reproducing our results are available at our GitHub page https://github.com/EyringMLClimateGroup/grundner25_iconaml_automatic_tuning/tree/main and preserved at <https://doi.org/10.5281/zenodo.15194060>.

Acknowledgements

A.G., J.S., M.S., and V.E. received funding for this study from the European Research Council (ERC) Synergy Grant “Understanding and modeling the Earth System with Machine Learning (USMILE)” under the Horizon 2020 research and innovation programme (Grant agreement No. 855187) and from the Horizon Europe project “Artificial Intelligence for enhanced representation of processes and extremes in Earth System Models (AI4PEX)” (Grant agreement ID:

101137682). T.B. received support from AIPEX, funded by the Swiss State Secretariat for Education, Research and Innovation (SERI, Grant No. 23.00546). V.E. was additionally supported by the Deutsche Forschungsgemeinschaft (DFG, German Research Foundation) through the Gottfried Wilhelm Leibniz Prize awarded to V.E. (reference no. EY 22/2-1). This work used resources of the Deutsches Klimarechenzentrum (DKRZ) granted by its Scientific Steering Committee (WLA) under project ID bd1179.

Author contributions

A.G., T.B. and V.E. designed the research; A.G. and J.S. performed the research and analyzed the data; A.L. and M.S. created the concept and ESMValTool code used for the evaluation of the simulations; A.G. wrote the paper with contributions from all co-authors.

Competing interests

The authors declare no conflict of interest.

References

- ¹ David J. Stensrud. *Parameterization Schemes: Keys to Understanding Numerical Weather Prediction Models*. Cambridge University Press, 2009.
- ² Veronika Eyring, William D Collins, Pierre Gentine, Elizabeth A Barnes, Marcelo Barreiro, Tom Beucler, Marc Bocquet, Christopher S Bretherton, Hannah M Christensen, Katherine Dagon, et al. Pushing the frontiers in climate modelling and analysis with machine learning. *Nature Climate Change*, 14(9):916–928, 2024.
- ³ Veronika Eyring, Pierre Gentine, Gustau Camps-Valls, David M. Lawrence, and Markus Reichstein. Ai-empowered next-generation multiscale climate modelling for mitigation and adaptation. *Nat. Geosci.*, 17:963–971, 2024. doi: <https://doi.org/10.1038/s41561-024-01527-w>.
- ⁴ Pierre Gentine, Mike Pritchard, Stephan Rasp, Gael Reinaudi, and Galen Yacalis. Could machine learning break the convection parameterization deadlock? *Geophysical Research Letters*, 45 (11):5742–5751, 2018.
- ⁵ Arthur Grundner, Tom Beucler, Pierre Gentine, Fernando Iglesias-Suarez, Marco A Giorgetta, and Veronika Eyring. Deep learning based cloud cover parameterization for icon. *Journal of Advances in Modeling Earth Systems*, 14(12):e2021MS002959, 2022.
- ⁶ Helge Heuer, Mierk Schwabe, Pierre Gentine, Marco A Giorgetta, and Veronika Eyring. Interpretable multiscale machine learning-based parameterizations of convection for icon. *Journal of Advances in Modeling Earth Systems*, 16(8):e2024MS004398, 2024.

⁷ Paul A O’Gorman and John G Dwyer. Using machine learning to parameterize moist convection: Potential for modeling of climate, climate change, and extreme events. *Journal of Advances in Modeling Earth Systems*, 10(10):2548–2563, 2018.

⁸ Stephan Rasp, Michael S Pritchard, and Pierre Gentine. Deep learning to represent subgrid processes in climate models. *Proceedings of the National Academy of Sciences*, 115(39):9684–9689, 2018. doi: 10.1073/pnas.1810286115.

⁹ Markus Reichstein, Gustau Camps-Valls, Bjorn Stevens, Martin Jung, Joachim Denzler, Nuno Carvalhais, and F Prabhat. Deep learning and process understanding for data-driven earth system science. *Nature*, 566(7743):195–204, 2019.

¹⁰ Arthur Grundner. *Data-driven cloud cover parameterizations for the ICON earth system model using deep learning and symbolic regression*. PhD thesis, Universität Bremen, January 25 2024. URL <https://media.suub.uni-bremen.de/handle/elib/7739>. Accessed: 2024-10-16.

¹¹ Annalisa Bracco, Julien Brajard, Henk A Dijkstra, Pedram Hassanzadeh, Christian Lessig, and Claire Monteleoni. Machine learning for the physics of climate. *Nature Reviews Physics*, 7(1):6–20, 2025.

¹² Hugo Frezat, Julien Le Sommer, Ronan Fablet, Guillaume Balarac, and Redouane Lguensat. A posteriori learning for quasi-geostrophic turbulence parametrization. *Journal of Advances in Modeling Earth Systems*, 14(11):e2022MS003124, 2022.

¹³ Costa Christopoulos, Ignacio Lopez-Gomez, Tom Beucler, Yair Cohen, Charles Kawczynski, Oliver R. A. Dunbar, and Tapio Schneider. Online learning of entrainment closures in a hybrid machine learning parameterization. *Journal of Advances in Modeling Earth Systems*, 16(11):e2024MS004485, 2024. doi: <https://doi.org/10.1029/2024MS004485>. URL <https://agupubs.onlinelibrary.wiley.com/doi/abs/10.1029/2024MS004485> e2024MS004485 2024MS004485.

¹⁴ Guoxing Chen, Wei-Chyung Wang, Shixi Yang, Yixin Wang, Feng Zhang, and Kun Wu. A neural network-based scale-adaptive cloud-fraction scheme for gcms. *Journal of Advances in Modeling Earth Systems*, 15(6):e2022MS003415, 2023.

¹⁵ Cyril Julien Morcrette, Tobias Cave, Helena Reid, Joana D da Silva Rodrigues, Teo Deveney, Lisa Kreusser, Kwinten Van Weverberg, and Chris Budd. Scale-aware parameterization of cloud fraction and condensate for a global atmospheric model machine-learnt from coarse-grained kilometer-scale simulations. *Authorea Preprints*, 2024.

¹⁶ Stephan Rasp. The optimization dichotomy: Why is it so hard to improve climate models with machine learning?, 2021. URL <https://raspstephan.github.io/blog/optimization-dichotomy/>. Accessed: 2024-10-16.

¹⁷ Arthur Grundner, Tom Beucler, Pierre Gentine, and Veronika Eyring. Data-driven equation discovery of a cloud cover parameterization. *Journal of Advances in Modeling Earth Systems*, 16(3):e2023MS003763, 2024.

¹⁸ Miles Cranmer. Interpretable machine learning for science with pysr and symbolic regression. *jl. arXiv preprint arXiv:2305.01582*, 2023.

¹⁹ Chris Huntingford, Andrew J Nicoll, Cornelia Klein, and Jawairia A Ahmad. Potential for equation discovery with ai in the climate sciences. *Earth System Dynamics*, 16(2):475–495, 2025.

²⁰ Ching-Yao Lai, Pedram Hassanzadeh, Aditi Sheshadri, Maike Sonnewald, Raffaele Ferrari, and Venkatramani Balaji. Machine learning for climate physics and simulations. *Annual Review of Condensed Matter Physics*, 16, 2024.

²¹ M. A. Giorgetta, T. Crueger, R. Brokopf, M. Esch, S. Fiedler, C. Hohenegger, L. Kornblueh, T. Mauritsen, C. Nam, A. K. Naumann, K. Peters, S. Rast, E. Roeckner, M. Sakradzija, H. Schmidt, J. Vial, R. Vogel, and B. Stevens. Icon-a, the atmosphere component of the icon earth system model: I. model description. *Journal of Advances in Modeling Earth Systems*, 10 (7):1638–1662, 2018. ISSN 1942-2466 1942-2466. doi: 10.1029/2017ms001233.

²² J David Neelin, Annalisa Bracco, Hao Luo, James C McWilliams, and Joyce E Meyerson. Considerations for parameter optimization and sensitivity in climate models. *Proceedings of the National Academy of Sciences*, 107(50):21349–21354, 2010.

²³ Shaocheng Xie, Hsi-Yen Ma, James S Boyle, Stephen A Klein, and Yuying Zhang. On the correspondence between short-and long-time-scale systematic errors in cam4/cam5 for the year of tropical convection. *Journal of Climate*, 25(22):7937–7955, 2012.

²⁴ Pauline Bonnet, Lorenzo Pastori, Mierk Schwabe, Marco A Giorgetta, Fernando Iglesias-Suarez, and Veronika Eyring. Tuning a climate model with machine-learning based emulators and history matching. *EGUsphere*, 2024:1–32, 2024.

²⁵ Lettie A Roach, Simon FB Tett, Michael J Mineter, Kuniko Yamazaki, and Cameron D Rae. Automated parameter tuning applied to sea ice in a global climate model. *Climate dynamics*, 50: 51–65, 2018.

²⁶ Veronika Eyring, Sandrine Bony, Gerald A Meehl, Catherine A Senior, Bjorn Stevens, Ronald J Stouffer, and Karl E Taylor. Overview of the Coupled Model Intercomparison Project Phase 6 (CMIP6) experimental design and organization. *Geoscientific Model Development*, 9(5):1937–1958, 2016.

²⁷ M. Righi, B. Andela, V. Eyring, A. Lauer, V. Predoi, M. Schlund, J. Vegas-Regidor, L. Bock, B. Brötz, L. de Mora, F. Diblen, L. Dreyer, N. Drost, P. Earnshaw, B. Hassler, N. Koldunov, B. Little, S. Loosveldt Tomas, and K. Zimmermann. Earth System Model Evaluation Tool (ESM-ValTool) v2.0 – technical overview. *Geoscientific Model Development*, 13(3):1179–1199, 2020. doi: 10.5194/gmd-13-1179-2020. URL <https://gmd.copernicus.org/articles/13/1179/2020/>.

²⁸ V. Eyring, L. Bock, A. Lauer, M. Righi, M. Schlund, B. Andela, E. Arnone, O. Bellprat, B. Brötz, L.-P. Caron, N. Carvalhais, I. Cionni, N. Cortesi, B. Crezee, E. L. Davin, P. Davini, K. Debeire, L. de Mora, C. Deser, D. Docquier, P. Earnshaw, C. Ehbrecht, B. K. Gier, N. Gonzalez-

Reviriego, P. Goodman, S. Hagemann, S. Hardiman, B. Hassler, A. Hunter, C. Kadow, S. Kindermann, S. Koirala, N. Koldunov, Q. Lejeune, V. Lembo, T. Lovato, V. Lucarini, F. Massonnet, B. Müller, A. Pandde, N. Pérez-Zanón, A. Phillips, V. Predoi, J. Russell, A. Seller, F. Serva, T. Stacke, R. Swaminathan, V. Torralba, J. Vegas-Regidor, J. von Hardenberg, K. Weigel, and K. Zimmermann. Earth System Model Evaluation Tool (ESMValTool) v2.0 – an extended set of large-scale diagnostics for quasi-operational and comprehensive evaluation of Earth system models in CMIP. *Geoscientific Model Development*, 13(7):3383–3438, 2020. doi: 10.5194/gmd-13-3383-2020. URL <https://gmd.copernicus.org/articles/13/3383/2020/>.

²⁹ A. Lauer, V. Eyring, O. Bellprat, L. Bock, B. K. Gier, A. Hunter, R. Lorenz, N. Pérez-Zanón, M. Righi, M. Schlund, D. Senftleben, K. Weigel, and S. Zechlau. Earth System Model Evaluation Tool (ESMValTool) v2.0 – diagnostics for emergent constraints and future projections from Earth system models in CMIP. *Geoscientific Model Development*, 13(9):4205–4228, 2020. doi: 10.5194/gmd-13-4205-2020. URL <https://gmd.copernicus.org/articles/13/4205/2020/>.

³⁰ K. Weigel, L. Bock, B. K. Gier, A. Lauer, M. Righi, M. Schlund, K. Adeniyi, B. Andela, E. Arnone, P. Berg, L.-P. Caron, I. Cionni, S. Corti, N. Drost, A. Hunter, L. Lledó, C. W. Mohr, A. Paçal, N. Pérez-Zanón, V. Predoi, M. Sandstad, J. Sillmann, A. Sterl, J. Vegas-Regidor, J. von Hardenberg, and V. Eyring. Earth System Model Evaluation Tool (ESMValTool) v2.0 – diagnostics for extreme events, regional and impact evaluation, and analysis of Earth system models in CMIP. *Geoscientific Model Development*, 14(6):3159–3184, 2021. doi: 10.5194/gmd-14-3159-2021. URL <https://gmd.copernicus.org/articles/14/3159/2021/>.

³¹ Bouwe Andela, Bjoern Broetz, Lee de Mora, Niels Drost, Veronika Eyring, Nikolay Koldunov, Axel Lauer, Valeriu Predoi, Mattia Righi, Manuel Schlund, Javier Vegas-Regidor, Klaus Zimmermann, Lisa Bock, Faruk Diblen, Laura Dreyer, Paul Earnshaw, Birgit Hassler, Bill Little, Saskia Loosveldt-Tomas, Stef Smeets, Jaro Camphuijsen, Bettina K. Gier, Katja Weigel, Mathias Hauser, Peter Kalverla, Evgenia Galytska, Pep Cos-Espuña, Inti Pelupessy, Sujan Koirala, Tobias Stacke, Sarah Alidoost, Martin Jury, Stéphane Sénési, Thomas Crocker, Barbara Vreede, Abel Soares Siqueira, Rémi Kazeroni, David Hohn, Julian Bauer, Romain Beucher, Jörg Benke, Eneko Martin-Martinez, and Diego Cammarano. ESMValCore, July 2024. URL <https://doi.org/10.5281/zenodo.3387139>.

³² Bouwe Andela, Bjoern Broetz, Lee de Mora, Niels Drost, Veronika Eyring, Nikolay Koldunov, Axel Lauer, Benjamin Mueller, Valeriu Predoi, Mattia Righi, Manuel Schlund, Javier Vegas-Regidor, Klaus Zimmermann, Kemisola Adeniyi, Enrico Arnone, Omar Bellprat, Peter Berg, Lisa Bock, Alejandro Bodas-Salcedo, Louis-Philippe Caron, Nuno Carvalhais, Irene Cionni, Nicola Cortesi, Susanna Corti, Bas Crezee, Edouard Leopold Davin, Paolo Davini, Clara Deser, Faruk Diblen, David Docquier, Laura Dreyer, Carsten Ehbrecht, Paul Earnshaw, Bettina Gier, Nube Gonzalez-Reviriego, Paul Goodman, Stefan Hagemann, Catherine Hardacre, Jost von Hardenberg, Birgit Hassler, Helge Heuer, Alasdair Hunter, Christopher Kadow, Stephan Kindermann, Sujan Koirala, Birgit Kuehbacher, Llorenç Lledó, Quentin Lejeune, Valerio Lembo, Bill

Little, Saskia Loosveldt-Tomas, Ruth Lorenz, Tomas Lovato, Valerio Lucarini, François Mas-sonnet, Christian Wilhelm Mohr, Pandde Amarjiit, Núria Pérez-Zanón, Adam Phillips, Joellen Russell, Marit Sandstad, Alistair Sellar, Daniel Senftleben, Federico Serva, Jana Sillmann, Tobias Stacke, Ranjini Swaminathan, Verónica Torralba, Katja Weigel, Ellen Sarauer, Charles Roberts, Peter Kalverla, Sarah Alidoost, Stefan Verhoeven, Barbara Vreede, Stef Smeets, Abel Soares Siqueira, Rémi Kazeroni, Jerry Potter, Franziska Winterstein, Romain Beucher, Jeremy Kraft, Lukas Ruhe, Pauline Bonnet, and Gregory Munday. ESMValTool, July 2024. URL <https://doi.org/10.5281/zenodo.3401363>.

³³ Axel Lauer, Lisa Bock, Birgit Hassler, Patrick Jöckel, Lukas Ruhe, and Manuel Schlund. Monitoring and benchmarking earth system model simulations with esmvaltool v2. 12.0. *Geoscientific Model Development*, 18(4):1169–1188, 2025.

³⁴ Manuel Schlund, Birgit Hassler, Axel Lauer, Bouwe Andela, Patrick Jöckel, Rémi Kazeroni, Saskia Loosveldt Tomas, Brian Medeiros, Valeriu Predoi, Stéphane Sénési, Jérôme Servonnat, Tobias Stacke, Javier Vegas-Regidor, Klaus Zimmermann, and Veronika Eyring. Evaluation of native Earth system model output with ESMValTool v2.6.0. *Geoscientific Model Development*, 16(1):315–333, 2023. doi: 10.5194/gmd-16-315-2023.

³⁵ Ronald Gelaro, Will McCarty, Max J Suárez, Ricardo Todling, Andrea Molod, Lawrence Takacs, Cynthia A Randles, Anton Darmenov, Michael G Bosilovich, Rolf Reichle, et al. The modern-era retrospective analysis for research and applications, version 2 (merra-2). *Journal of climate*, 30(14):5419–5454, 2017.

³⁶ Norman G Loeb, David R Doelling, Hailan Wang, Wenying Su, Cathy Nguyen, Joseph G Corbett, Lusheng Liang, Cristian Mitrescu, Fred G Rose, and Seiji Kato. Clouds and the earth's radiant energy system (ceres) energy balanced and filled (ebaf) top-of-atmosphere (toa) edition-4.0 data product. *Journal of climate*, 31(2):895–918, 2018.

³⁷ Yuanchong Zhang and William B Rossow. Global radiative flux profile data set: Revised and extended. *Journal of Geophysical Research: Atmospheres*, 128(5):e2022JD037340, 2023.

³⁸ Karl-Göran Karlsson, Kati Anttila, Jörg Trentmann, Martin Stengel, Irina Solodovnik, Jan Fokke Meirink, Abhay Devasthale, Steffen Kothe, Emmihenna Jääskeläinen, Joseph Sedlar, Nikos Benas, Gerd-Jan van Zadelhoff, Diana Stein, Stephan Finkensieper, Nina Håkansson, Rainer Hollmann, Johannes Kaiser, and Martin Werscheck. Clara-a2.1: Cm saf cloud, albedo and surface radiation dataset from avhrr data - edition 2.1, 2020. URL https://wui.cmsaf.eu/safira/action/viewDoiDetails?acronym=CLARA_AVHRR_V002_01.

³⁹ Martin Stengel, Stefan Stapelberg, Oliver Sus, Cornelia Schlundt, Caroline Poulsen, Gareth Thomas, Matthew Christensen, Cintia Carbajal Henken, Rene Preusker, Jürgen Fischer, et al. Cloud property datasets retrieved from avhrr, modis, aatsr and meris in the framework of the cloud_cci project. *Earth System Science Data*, 9(2):881–904, 2017.

⁴⁰ Steven Platnick, Michael D King, Steven A Ackerman, W Paul Menzel, Bryan A Baum, Jérôme C Riédi, and Richard A Frey. The modis cloud products: Algorithms and examples from terra. *IEEE Transactions on geoscience and Remote Sensing*, 41(2):459–473, 2003.

⁴¹ Andrew K Heidinger, Michael J Foster, Andi Walther, and Xuepeng Zhao. The pathfinder atmospheres–extended avhrr climate dataset. *Bulletin of the American Meteorological Society*, 95(6):909–922, 2014.

⁴² Hans Hersbach, Bill Bell, Paul Berrisford, Shoji Hirahara, András Horányi, Joaquín Muñoz-Sabater, Julien Nicolas, Carole Peubey, Raluca Radu, Dinand Schepers, et al. The era5 global reanalysis. *Quarterly Journal of the Royal Meteorological Society*, 146(730):1999–2049, 2020.

⁴³ Mark D Zelinka, Timothy A Myers, Daniel T McCoy, Stephen Po-Chedley, Peter M Caldwell, Paulo Ceppi, Stephen A Klein, and Karl E Taylor. Causes of higher climate sensitivity in cmip6 models. *Geophysical Research Letters*, 47(1):e2019GL085782, 2020.

⁴⁴ Andreas Muhlbauer, Isabel L McCoy, and Robert Wood. Climatology of stratocumulus cloud morphologies: microphysical properties and radiative effects. *Atmospheric Chemistry and Physics*, 14(13):6695–6716, 2014.

⁴⁵ Xinyan Liu, Tao He, Lin Sun, Xiongxin Xiao, Shunlin Liang, and Siwei Li. Analysis of daytime cloud fraction spatiotemporal variation over the arctic from 2000 to 2019 from multiple satellite products. *Journal of Climate*, 35(23):7595–7623, 2022.

⁴⁶ Spencer K Clark, Noah D Brenowitz, Brian Henn, Anna Kwa, Jeremy McGibbon, W Andre Perkins, Oliver Watt-Meyer, Christopher S Bretherton, and Lucas M Harris. Correcting a 200 km resolution climate model in multiple climates by machine learning from 25 km resolution simulations. *Journal of Advances in Modeling Earth Systems*, 14(9):e2022MS003219, 2022.

⁴⁷ Dmitrii Kochkov, Janni Yuval, Ian Langmore, Peter Norgaard, Jamie Smith, Griffin Mooers, Milan Klöwer, James Lottes, Stephan Rasp, Peter Düben, et al. Neural general circulation models for weather and climate. *Nature*, 632(8027):1060–1066, 2024.

⁴⁸ K. Marvel, M. Zelinka, S. A. Klein, C. Bonfils, P. Caldwell, C. Doutriaux, and K. E. Taylor. External influences on modeled and observed cloud trends. *Journal of Climate*, 28(12):4820–4840, 2015. doi: 10.1175/JCLI-D-14-00734.1.

⁴⁹ J. R. Norris, R. J. Allen, A. T. Evan, M. D. Zelinka, C. W. O’Dell, and S. A. Klein. Evidence for climate change in the satellite cloud record. *Nature*, 536(7614):72–75, 2016. doi: 10.1038/nature18273.

⁵⁰ Paulo Ceppi, Florent Brient, Mark D Zelinka, and Dennis L Hartmann. Cloud feedback mechanisms and their representation in global climate models. *Wiley Interdisciplinary Reviews: Climate Change*, 8(4):e465, 2017.

⁵¹ J. E. Kay, T. L’Ecuyer, H. Chepfer, N. Loeb, A. Morrison, and G. Cesana. Recent advances in arctic cloud and climate research. *Current Climate Change Reports*, 2:159–169, 2016. doi: 10.1007/s40641-016-0051-9.

⁵² A. L. Morrison, J. E. Kay, W. R. Frey, H. Chepfer, and R. Guzman. Cloud response to arctic sea ice loss and implications for future feedback in the cesm1 climate model. *Journal of Geophysical Research: Atmospheres*, 124(2):1003–1020, 2019. doi: 10.1029/2018JD029142.

⁵³ V. Mendoza, M. Pazos, R. Garduño, and B. Mendoza. Thermodynamics of climate change between cloud cover, atmospheric temperature and humidity. *Scientific Reports*, 11(1):21244, 2021. doi: 10.1038/s41598-021-00474-1.

⁵⁴ Thorsten Mauritsen, Bjorn Stevens, Erich Roeckner, Traute Crueger, Monika Esch, Marco Giorgetta, Helmuth Haak, Johann Jungclaus, Daniel Klocke, Daniela Matei, et al. Tuning the climate of a global model. *Journal of advances in modeling Earth systems*, 4(3), 2012.

⁵⁵ Hilding Sundqvist, Erik Berge, and Jón Egill Kristjánsson. Condensation and cloud parameterization studies with a mesoscale numerical weather prediction model. *Monthly Weather Review*, 1989.

⁵⁶ J. A. Nelder and R. Mead. A simplex method for function minimization. *The Computer Journal*, 7(4):308–313, 1965. doi: 10.1093/comjnl/7.4.308. URL <https://academic.oup.com/comjnl/article/7/4/308/354237>.

⁵⁷ R. F. Adler, M. R. Sapiano, G. J. Huffman, J. J. Wang, G. Gu, D. Bolvin, E. Nelkin, K. P. Bowman, Y. Hong, E. F. Stocker, and D. B. Shin. The global precipitation climatology project (gpcp) monthly analysis (new version 2.3) and a review of 2017 global precipitation. *Atmosphere*, 9(4):138, 2018. doi: 10.3390/atmos9040138. URL <https://www.mdpi.com/2073-4433/9/4/138>.

⁵⁸ A. Lauer, L. Bock, B. Hassler, M. Schröder, and M. Stengel. Cloud climatologies from global climate models—a comparison of cmip5 and cmip6 models with satellite data. *Journal of Climate*, 36(2):281–311, 2023. doi: 10.1175/JCLI-D-22-0181.1. URL <https://journals.ametsoc.org/view/journals/clim/36/2/JCLI-D-22-0181.1.xml>.

⁵⁹ Bjorn Stevens, Masaki Satoh, Ludovic Auger, Joachim Biercamp, Christopher S Bretherton, Xi Chen, Peter Düben, Falko Judt, Marat Khairoutdinov, Daniel Klocke, et al. Dyamond: the dynamics of the atmospheric general circulation modeled on non-hydrostatic domains. *Progress in Earth and Planetary Science*, 6(1):1–17, 2019.

⁶⁰ Claudia Christine Stephan, Julia Duras, Lucas Harris, Daniel Klocke, William M Putman, Mark Taylor, Nils Wedi, Nedjeljka Žagar, and Florian Ziemen. Atmospheric energy spectra in global kilometre-scale models. *Tellus A: Dynamic Meteorology and Oceanography*, 74(1), 2022.